A critical residue in the α_1M2–M3 linker regulating mammalian GABA$_A$ receptor pore gating by diazepam

Joseph W Nors, Shipra Gupta, Marcel P Goldschen-Ohm*

University of Texas at Austin, Department of Neuroscience, Austin, United States

Abstract Benzodiazepines (BZDs) are a class of widely prescribed psychotropic drugs that modulate activity of GABA$_A$ receptors (GABA$_A$Rs), neurotransmitter-gated ion channels critical for synaptic transmission. However, the physical basis of this modulation is poorly understood. We explore the role of an important gating domain, the α_1M2–M3 linker, in linkage between the BZD site and pore gate. To probe energetics of this coupling without complication from bound agonist, we use a gain of function mutant (α_1L9'T$\beta_2\gamma_{2L}$) directly activated by BZDs. We identify a specific residue whose mutation (α_1V279A) more than doubles the energetic contribution of the BZD positive modulator diazepam (DZ) to pore opening and also enhances DZ potentiation of GABA-evoked currents in a wild-type background. In contrast, other linker mutations have little effect on DZ efficiency, but generally impair unliganded pore opening. Our observations reveal an important residue regulating BZD-pore linkage, thereby shedding new light on the molecular mechanism of these drugs.

*For correspondence:
marcel.goldschen-ohm@austin.
utexas.edu

Competing interests: The authors declare that no competing interests exist.

Introduction

Benzodiazepines (BZDs) (e.g. Valium, Xanax) are one of the most widely prescribed psychotropic drugs today. An estimated nearly 100 million adults in the United States are prescribed a BZD annually (*Agarwal and Landon, 2019*; *Bachhuber et al., 2016*; *Olfson et al., 2015*). Their anxiolytic and sedative properties are used as therapies for conditions including anxiety, panic, insomnia, seizures, muscle spasms, pain, and alcohol withdrawal (*Möhler et al., 2002*). Although largely effective, BZDs have undesirable effects, including tolerance, addiction, dependence, and withdrawal symptoms, and are often co-abused with alcohol and opioids (*Fluyau et al., 2018*; *Schmitz, 2016*; *Jones and McAninch, 2015*; *Jones et al., 2010*). Novel therapies with reduced risks are imperative for safer long-term treatment options.

The therapeutic effects of BZDs are conferred upon binding to and modulating the activity of GABA$_A$Rs, which are the primary inhibitory neurotransmitter-gated ion channels in the central nervous system (*Smart and Stephenson, 2019*). GABA$_A$Rs are part of the Cys-loop superfamily of pentameric ligand-gated ion channels (pLGICs) including homologous glycine (Gly), nicotinic acetylcholine (nACh), serotonin type 3 (5-HT$_3$), and zinc-activated receptors as well as prokaryotic homologs (*Pless and Sivilotti, 2018*; *Nemecz et al., 2016*; *Tasneem et al., 2004*; *Connolly and Wafford, 2004*). Each pentameric GABA$_A$R is comprised of subtype-specific combinations of five homologous but nonidentical subunits (α_{1-6}, β_{1-3}, γ_{1-3}, δ, ϵ, π, θ, ρ_{1-3}) that together form a central chloride conducting pore (*Figure 1*; *Olsen and Sieghart, 2008*). The most prominent subtype at synapses is comprised of α_1, β_n, and γ_2 subunits (*Sieghart and Sperk, 2002*). GABA$_A$Rs provide a critical balance with excitatory signaling for normal neural function, and not surprisingly, their dysfunction is related to disorders such as epilepsy, autism spectrum disorder, intellectual disability, schizophrenia, and neurodevelopmental disorders such as fragile X syndrome (*Hernandez and Macdonald, 2019*; *Gao et al., 2018*; *Mahdavi et al., 2018*; *Braat and Kooy, 2015*; *Vien et al., 2015*;
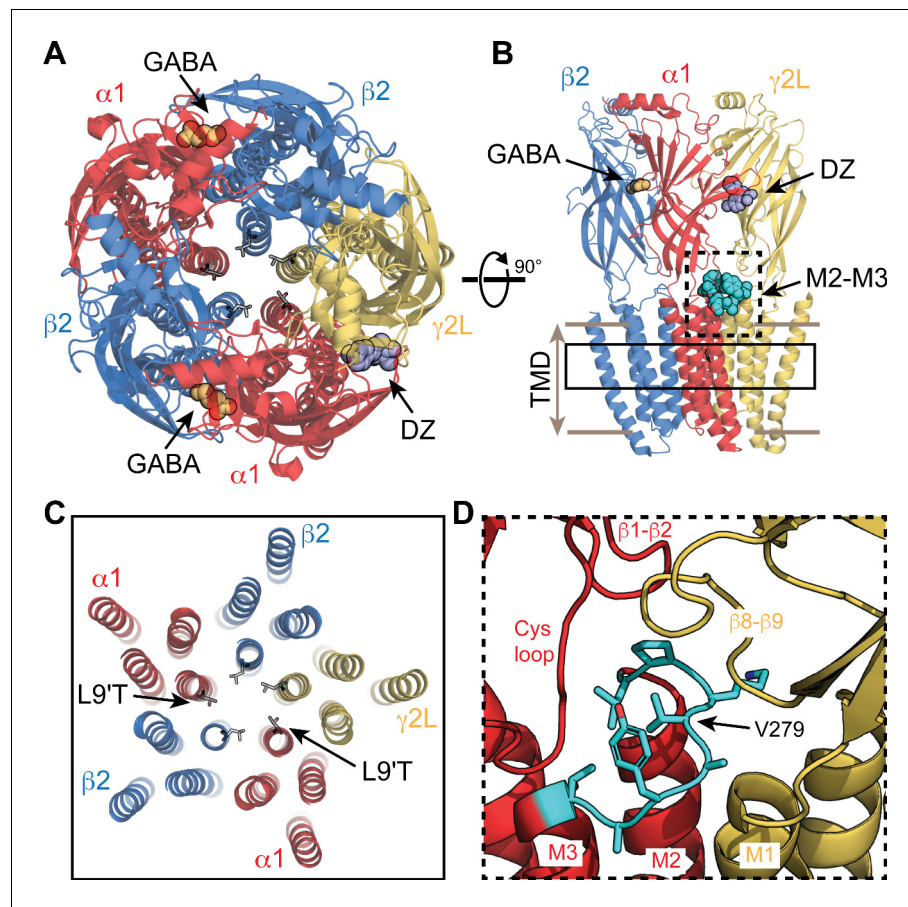
Figure 1. Visual representation of an $\alpha_1\beta_2\gamma_2$ GABA$_A$ receptor from cryo-EM map PDB 6X3X. (A,B) View from the extracellular space (A) and parallel to the membrane plane (B). Bound GABA and DZ are shown as gold and lavender spheres, respectively. The 9' pore residue from each subunit is shown in stick representation, all leucine except for the mutation α_1L9'T, which was generated in PyMol as a visualization aid. One of the two α_1M2–M3 linkers is shown as cyan spheres in (B). (C) Same view as in (A) for a slice through the transmembrane domains indicated by the solid box in (B). (D) Detail for the dashed box in (B). The α_1M2–M3 linker (L276-T283; rat numbering) is colored cyan with side chains shown in stick representation.

The online version of this article includes the following figure supplement(s) for figure 1:

Figure supplement 1. Sequence alignment of M2–M3 linker regions for subunits from several members of the pLGIC superfamily.

Rudolph and Möhler, 2014; Limon et al., 2012; Ramamoorthi and Lin, 2011; Solís-Añez et al., 2007). Although pharmacological manipulation of GABA$_A$Rs is a powerful approach to tuning neural signaling, the rational design of novel therapies is challenged by a lack of understanding of the molecular mechanism by which drugs such as BZDs modulate channel behavior.

In conjunction with structural models of mostly homomeric pLGICs, recent cryo-EM models of heteromeric GABA$_A$Rs with bound neurotransmitter and BZD provide an important conceptual aid to understand the mechanism of action of these drugs (Kim et al., 2020; Masiulis et al., 2019; Laverty et al., 2019; Phulera et al., 2018; Zhu et al., 2018). Consistent with earlier functional studies (Sigel and Ernst, 2018; Sigel and Lüscher, 2011; Sigel, 2002; Wagner and Czajkowski, 2001; Kucken et al., 2000; McKernan et al., 1998; Pritchett et al., 1989; Gibbs et al., 1985), they show that BZDs are bound at a specific recognition site in the extracellular domain between α and γ subunits (Figure 1). However, these structures have yet to clarify the mechanism by which BZDs modulate channel activity.

Kinetic models of interacting domains and thermodynamic linkage analysis can be used to estimate the energy of interaction between binding sites and the pore gate from bulk measures of

ensemble average activity (*Goldschen-Ohm et al., 2014*; *Chowdhury and Chanda, 2013*; *Wyman and Gill, 1990*). Coupled with mutagenesis or other perturbations, these interactions can be probed to elucidate their physical basis. However, these approaches are challenged for BZDs because they do not evoke robust channel opening by themselves, but instead modulate responses to an agonist such as GABA. Thus, typical experimental measures reflect channels with both agonist and BZD bound. This makes it difficult to dissect whether the drug has altered either agonist binding or channel gating as the two processes are intimately coupled (*Colquhoun, 1998*). This challenge has contributed to differing conclusions postulating that BZDs alter either agonist binding (*Goldschen-Ohm et al., 2010*; *Perrais and Ropert, 1999*; *Mellor and Randall, 1997*; *Rogers et al., 1994*; *Vicini et al., 1987*), pore gating (*Li et al., 2013*; *Downing et al., 2005*; *Campo-Soria et al., 2006*; *Rüsch and Forman, 2005*), or an intermediate preactivation step (*Goldschen-Ohm et al., 2014*; *Gielen et al., 2012*). The ability of BZDs to potentiate current responses to saturating concentrations of partial agonists, and also to directly gate gain of function mutants, implies that the drug's effect is not due to changes in binding alone. A combination of effects on both binding and gating as predicted by changes in intermediate gating steps energetically coupled with both binding sites and the pore gate is plausible (*Goldschen-Ohm et al., 2014*). However, the molecular identity of any such intermediate states remains unclear.

Here we examined linkage between the BZD site and pore gate in isolation from any effect of the drug on agonist binding using a spontaneously active gain of function mutant (α_1L9'T$\beta_2\gamma_{2L}$) that is directly gated by BZDs alone (*Scheller and Forman, 2002*; *Chang and Weiss, 1999*). In the α_1L9'T background, we serially mutated each residue in the α_1M2–M3 linker to alanine and assessed the effect on modulation of the channel pore by the BZD positive modulator DZ (Valium) in the absence of agonist. The M2–M3 linker is a loop following the pore lining M2 helix that together with several other important interfacial loops defines the region connecting extracellular ligand binding and transmembrane domains known to be crucially involved in the gating process of pLGICs (*Figure 1*). Structural models show that agonist binding is associated with an outward displacement of the M2–M3 linker from the central pore axis (*Nemecz et al., 2016*). Mutations in the linker generally impair gating by agonists (*Kash et al., 2003*; *O'Shea and Harrison, 2000*), and some are associated with genetic diseases such as epilepsy in GABA$_A$Rs (*Hales et al., 2006*; *Hernandez and Macdonald, 2019*) or hyperekplexia in GlyRs (*Bode and Lynch, 2014*). However, the role of the M2–M3 linker in drug modulation by BZDs is less understood.

We show that alanine substitutions throughout the α_1M2–M3 linker generally impair unliganded pore gating, whereas they have little effect on the efficiency by which chemical energy from DZ binding is transmitted to the pore gate. The notable exception is α_1V279A, which more than doubles DZ's energetic contribution to pore opening, whereas larger side chains at this site do not. In a wild-type background, α_1V279A enhances DZ potentiation of currents evoked by even saturating GABA, consistent with a direct effect on the pore closed/open equilibrium. Our observations identify an important residue in the α_1M2–M3 linker regulating the efficiency of BZD modulation in GABA$_A$Rs.

Results

Alanine substitutions in the α_1M2–M3 linker generally impair unliganded gating

We use the gain of function mutation α_1L9'T that confers spontaneous channel gating in the absence of agonist that can be further modulated by BZDs (*Scheller and Forman, 2002*; *Chang and Weiss, 1999*). The primary purpose for this mutation is to enable macroscopic current responses to report on pore gating by a BZD in the absence of agonist. Initially, we examine unliganded and GABA-evoked gating and in later sections turn to BZDs. In the α_1L9'T$\beta_2\gamma_{2L}$ (α_1L9'T or L9'T) gain of function background, we assessed the effects of alanine substitutions in the α_1M2–M3 linker on unliganded and GABA-evoked channel activity. We restricted the scan primarily to the flexible loop between helical regions associated with M2 and M3 from α_1L276-T283 (*Figure 1*; *Figure 1—figure supplement 1*). Two of these positions, α_1A280 and α_1A282, are natively alanine and were not mutated. Briefly, *Xenopus laevis* oocytes were co-injected with mRNA for α, β, and γ subunits in a 1:1:10 ratio, and current responses to microfluidic application of ligands were recorded in two-electrode voltage clamp. Each recording consisted of a series of 10 second pulses of GABA at various concentrations
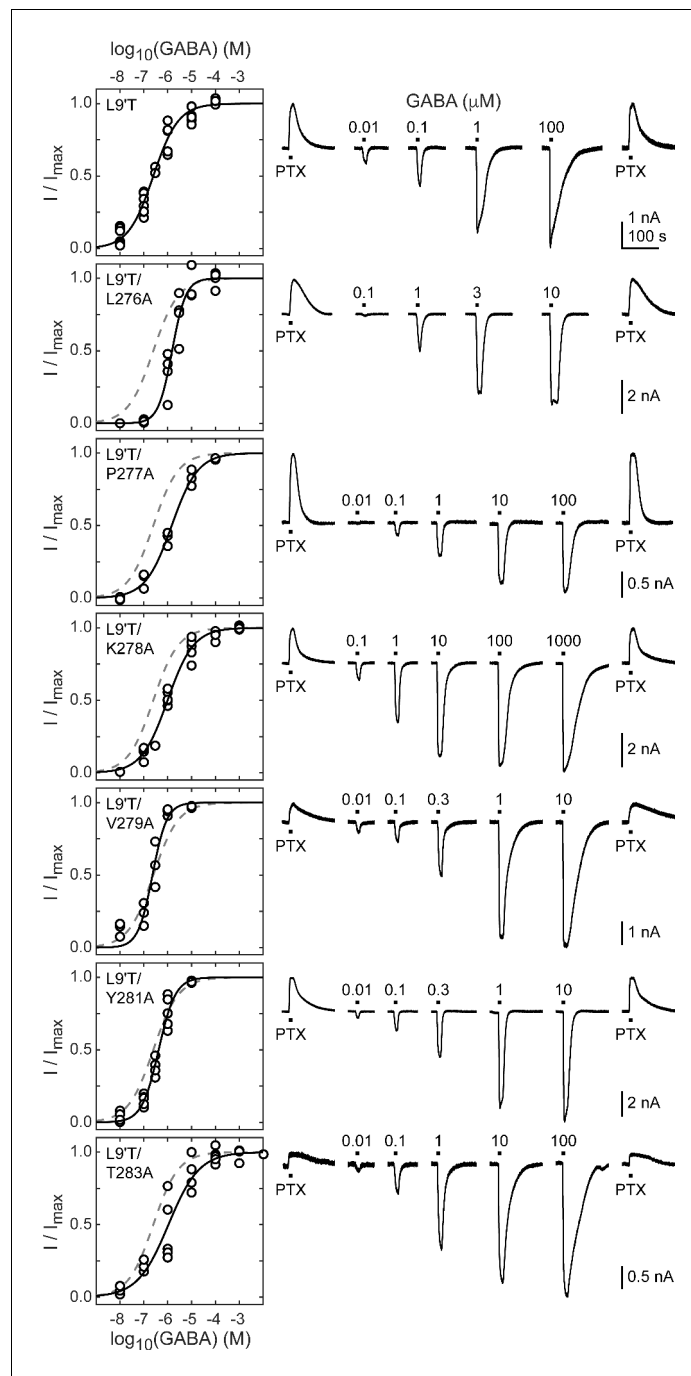
Figure 2. Spontaneous PTX-sensitive and GABA-evoked currents for α_1M2–M3 linker alanine substitutions in the gain of function α_1L9'T$\beta_2\gamma_{2L}$ background. (Left) Summary of normalized GABA concentration–response relationships for GABA-evoked currents with the zero current baseline set to the level of spontaneous activity. Solid line is a fit of the pooled data across oocytes to *Equation 1*, and the dashed line is the fit for the L9'T background. Fit parameters are EC$_{50}$, hill slope (# oocytes): L9'T = 0.25 μM, 0.83 (7); L9'T/L276A = 1.53 μM, 1.51 (4); L9'T/P277A = 1.48 μM, 0.80 (3); L9'T/K278A = 0.99 μM, 0.79 (5); L9'T/V279A = 0.23 μM, 1.44 (4); L9'T/Y281A = 0.42 μM, 1.23 (5); L9'T/T283A = 1.08 μM, 0.67 (5). Parameters for fits to individual oocytes are summarized in *Figure 2—figure supplement 2*. (Right) Example currents in response to 10 second pulses of the pore blocker PTX (1 mM) or GABA (concentration in micromolar indicated above each pulse). Responses to GABA were bookended by application of PTX to assess the amount of spontaneous current and to normalize any drift or rundown during the experiment (see *Figure 2—figure supplement 1*).

The online version of this article includes the following figure supplement(s) for figure 2:

Figure 2 continued on next page

Figure 2 continued

Figure supplement 1. Correction for baseline drift and current rundown.
Figure supplement 2. Summary of GABA EC$_{50}$ and hill slope from fitting *Equation 1* to GABA concentration–response relationships as shown in *Figure 2* for individual oocytes.
Figure supplement 3. Responses of wild-type $\alpha_1\beta_2\gamma_{2L}$ receptors to 10 second pulses of either 1 mM PTX, 3 μM DZ, or 3 mM GABA.

---

bookended by 10 second pulses of 1 mM picrotoxin (PTX) (*Figure 2*). Current block by the pore blocker PTX was used to assess the amount of spontaneous activity and to correct for drift or rundown over the course of the experiment (see *Figure 2—figure supplement 1*). In comparison, wild-type receptors have little to no PTX-sensitive spontaneous activity (*Figure 2—figure supplement 3*). Normalized concentration–response relationships for the additional GABA-evoked current above the spontaneous current baseline in the L9'T background are shown in *Figure 2*. As compared to α_1L9'T, all of the alanine mutations exhibited an increase in the EC$_{50}$ and/or steepness of the GABA concentration–response relationship (*Figure 2*; *Figure 2—figure supplement 2*). The increased EC$_{50}$ is generally consistent with previous reports of α_1M2–M3 linker mutations in a wild-type background (*O'Shea and Harrison, 2000*) and implies that side chain interactions in this region are important for channel gating by agonists. The steepness of the concentration–response relationship for α_1L9'T was fairly shallow, with a hill slope slightly below one. This could reflect an increased efficiency of mono-liganded gating in the gain of function background. In such a case, the steeper hill slopes conferred by α_1L276A, α_1V279A, and α_1Y281A may be due to a reduction in the efficiency of mono- vs di-liganded gating, although this was not verified.

The level of unliganded channel activity was determined from the ratio of the spontaneous current amplitude as assessed by block with PTX (I$_{PTX}$) to the maximal current amplitude evoked with saturating GABA (I$_{GABA-max}$) (*Figure 3A*). The unliganded open probability was estimated as the product of the ratio I$_{PTX}$/I$_{GABA-max}$ and the open probability in saturating GABA (P$_{o-GABA-max}$). Under the assumption that P$_{o-GABA-max}$ is similar for all constructs, all α_1M2–M3 linker mutations except for α_1P277A reduced the unliganded open probability by approximately two-fold (*Figure 3B*, *Table 1*). P$_{o-GABA-max}$ is ~0.85 in wild-type channels (*Keramidas and Harrison, 2010*), and likely to be closer to 1.0 in a gain of function background such as α_1L9'T that is further known to desensitize much more slowly than wild-type (*Scheller and Forman, 2002*). This assumption was verified for single
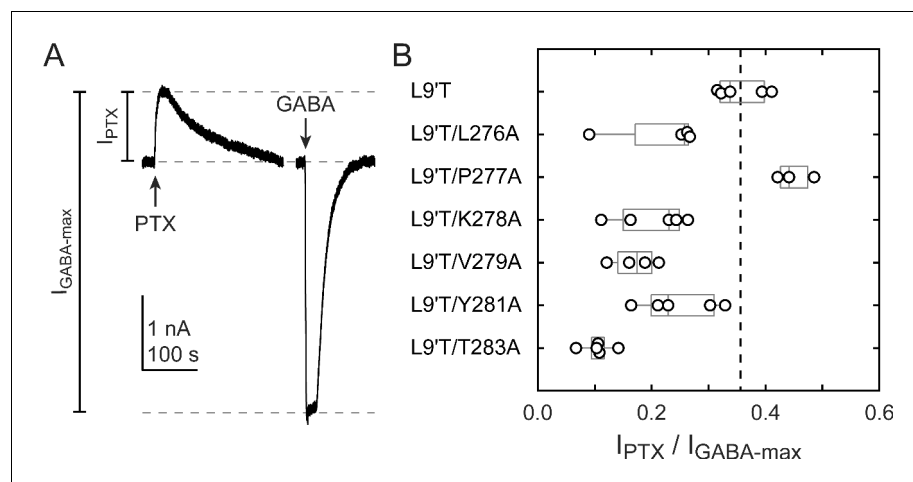

Figure 3. Ratio of PTX-sensitive to maximal GABA-evoked current amplitude. (A) Example currents from α_1L9'T/V279A$\beta_2\gamma_{2L}$ receptors elicited by 10 second pulses of either 1 mM PTX or 10 μM GABA. (B) Summary of the ratio of PTX-sensitive to maximal GABA-evoked current amplitude for individual oocytes. Gray box plots indicate the median and 25th and 75th percentiles. The vertical dashed line is the mean for L9'T. These ratios were estimated as being approximately proportional to the unliganded open probability by a factor that is the open probability in saturating GABA.

Table 1. Summary of peak current ratios and $\Delta\Delta G_{DZ}$ for mutations in the L9'T background. Data are mean ± standard deviation (# oocytes), and individual data points are shown in *Figures 3B*, *5B*, *6C,* and *7C*.

	$I_{PTX}/I_{GABA-max}$	I_{DZ-max}/I_{PTX}	$\Delta\Delta G_{DZ}$ (kcal/mol)
L9'T	0.36 ± 0.04 (5)	1.35 ± 0.05 (5)	−0.31 ± 0.04 (5)
L9'T/L276A	0.22 ± 0.09 (4)	1.62 ± 0.07 (5)	−0.45 ± 0.04 (5)
L9'T/P277A	0.45 ± 0.03 (3)	1.41 ± 0.17 (5)	−0.46 ± 0.20 (5)
L9'T/K278A	0.20 ± 0.06 (5)	1.67 ± 0.15 (4)	−0.44 ± 0.08 (4)
L9'T/V279A	0.17 ± 0.04 (4)	3.30 ± 0.70 (5)	−1.11 ± 0.30 (5)
L9'T/V279D	0.02 ± 0.005 (3)	2.31 ± 0.08 (3)	−0.52 ± 0.02 (3)
L9'T/V279W	0.16 ± 0.05 (2)	1.96 ± 0.23 (3)	−0.53 ± 0.10 (3)
L9'T/Y281A	0.25 ± 0.07 (5)	1.59 ± 0.11 (4)	−0.42 ± 0.07 (4)
L9'T/T283A	0.11 ± 0.03 (5)	1.71 ± 0.10 (6)	−0.38 ± 0.04 (6)

L9'T/V279A receptors (*Figure 7—figure supplement 1*). Thus, any reduction in $P_{o-GABA-max}$ for the linker mutations should only further reduce their estimated unliganded open probability. In summary, these data show that alanine mutations in the α_1M2–M3 linker generally impair channel gating by increasing GABA EC_{50} and/or reducing unliganded pore opening. This suggests that α_1M2–M3 linker side chain interactions play an important role in the closed vs. open pore equilibrium even in the absence of agonist.

All but one alanine substitution in the α_1M2–M3 linker have little effect on activation by DZ relative to unliganded activity

BZD positive modulators alone evoke channel opening with extremely low probability (*Campo-Soria et al., 2006*), thus necessitating coapplication with an agonist to obtain robust currents from wild-type receptors (*Germann et al., 2019*). However, dissecting the effects of BZDs on either agonist binding or channel gating is severely challenged in the presence of an agonist because the two processes are intimately coupled (*Colquhoun, 1998*). To isolate effects on gating apart from any effects on agonist binding, we examined the effect of alanine substitutions in the α_1M2–M3 linker on DZ-evoked currents in the background of the gain of function mutation α_1L9'T in the absence of agonist. Concentration–response relationships for currents evoked by 10 second pulses of DZ were bookended by 10 second pulses of 1 mM PTX to assess spontaneous activity (*Figure 4*). Drift or rundown was corrected as described for GABA-evoked currents (*Figure 2—figure supplement 1*). Normalized concentration–response relationships for the additional DZ-elicited current above the spontaneous current baseline were fit to *Equation 1*. Alanine substitutions in the α_1M2–M3 linker have no obvious effect on DZ concentration–response relationships with the exception of α_1L276A that confers a right shift and reduction in steepness (*Figure 4*; *Figure 4—figure supplement 1*). Reports for the EC_{50} of DZ potentiation in wild-type receptors are similar to the DZ EC_{50} for α_1L9'T receptors reported here and in previous studies (*Li et al., 2013*; *Campo-Soria et al., 2006*; *Rüsch and Forman, 2005*; *Walters et al., 2000*).

The ratio of the maximal DZ-evoked current amplitude (I_{DZ-max}) to PTX-sensitive current amplitude (I_{PTX}) is a measure for how well DZ activates the channel relative to its spontaneous unliganded activity. This ratio is largely independent of alanine substitution in the α_1M2–M3 linker with the notable exception of α_1V279A (*Figure 5*, Table 1). Thus, apart from α_1V279A, DZ-evoked currents are predictably proportional to the amount of unliganded activity. This suggests that α_1V279 has a unique role in DZ modulation, whereas side chains of other linker residues are involved little or not at all.

Dependence of DZ gating on charge and volume at α_1V279

The M2–M3 linker has both high sequence and structural similarity in pLGICs. The valine at position 279 in the $GABA_A R$ α_1 subunit is located near the center of the linker and is nearly always an aliphatic residue in different $GABA_A R$ subunits as well as in subunits of other pLGICs, with the exception of AChR, where it is a threonine. Even where sequences differ, structural models of the M2–M3
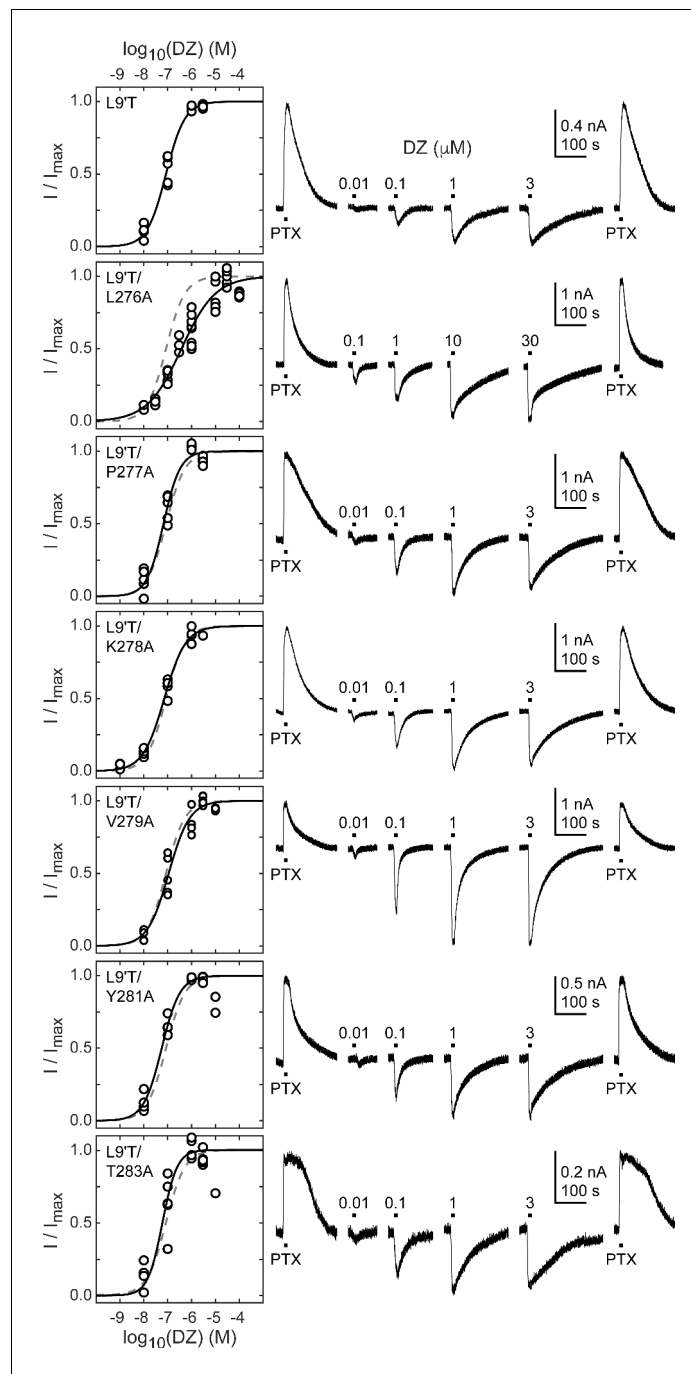
Figure 4. Spontaneous PTX-sensitive and DZ-evoked currents for α_1M2–M3 linker alanine substitutions in the gain of function α_1L9'T$\beta_2\gamma_{2L}$ background. (Left) Summary of normalized DZ concentration–response relationships for DZ-evoked currents with the zero current baseline set to the level of spontaneous activity. Solid line is a fit of the pooled data across oocytes to *Equation 1*, and the dashed line is the fit for the L9'T background. Reduced peak responses to 10 μM DZ for L9'T/Y281A and L9'T/T283A were omitted from the fits. Fit parameters are EC_{50}, hill slope (# oocytes): L9'T = 85 nM, 1.10 (5); L9'T/L276A = 380 nM, 0.61 (8); L9'T/P277A = 67 nM, 1.24 (5); L9'T/K278A = 72 nM, 0.97 (4); L9'T/V279A = 110 nM, 0.98 (5); L9'T/Y281A = 56 nM, 1.14 (4); L9'T/T283A = 60 nM, 1.42 (6). Parameters for fits to individual oocytes are summarized in *Figure 4—figure supplement 1*. (Right) Example currents in response to 10 second pulses of the pore blocker PTX (1 mM) or DZ (concentration in micromolar indicated above each pulse). Responses to DZ were bookended by application of PTX to assess the amount of spontaneous current and to normalize any drift or rundown during the experiment (see *Figure 2—figure supplement 1*).

Figure 4 continued on next page

Figure 4 continued

The online version of this article includes the following figure supplement(s) for figure 4:

Figure supplement 1. Summary of DZ EC_{50} and hill slope from fitting *Equation 1* to DZ concentration–response relationships as shown in *Figure 4* for individual oocytes.

---

linker for multiple pLGICs are highly similar. To explore the side chain properties relevant to DZ gating, we examined the effect of introducing a charged aspartate or bulky tryptophan at position 279 in the α_1L9'T background. We recorded unliganded PTX-sensitive and GABA- or DZ-evoked currents as described above and compared their relative current amplitudes and concentration–response relationships (*Figure 6*). The negative charge introduced by α_1V279D severely inhibits unliganded gating, exhibiting very little PTX-sensitive current in relation to robust currents evoked with saturating GABA. In contrast, addition of the bulky side chain α_1V279W only slightly impairs unliganded gating to a similar degree as substitution with alanine. These data suggest that side chain volume at this position is less critical for unliganded gating, whereas introduction of a negative charge nearly abolishes spontaneous activity despite the α_1L9'T pore mutation. Consistent with impaired pore gating, α_1V279D increases the GABA EC_{50} by ~100-fold.

The ratio of DZ-evoked to PTX-sensitive current amplitude is only slightly increased by α_1V279W, whereas it is further increased by α_1V279D, albeit not to the extent of α_1V279A (*Figure 6C*). However, we were unable to reach saturation for DZ-evoked currents from α_1V279D due to a reduction in peak current amplitude at higher DZ concentrations consistent with occupation of a secondary lower affinity inhibitory site (*Figure 6B*). Thus, our observations for α_1V279D reflect a lower limit on channel activity evoked by DZ binding. Even if α_1V279D has an appreciable effect on the ratio of DZ-evoked to unliganded current, the overall effect of this mutation on channel function is likely to be dominated by its inhibition of pore gating. In contrast, α_1V279W has similar effects to alanine substitutions at other linker residues. These data suggest that DZ gating is specifically enhanced by a reduction of side chain volume at position 279.

The mutation α_1V279A increases DZ's energetic contribution to pore gating

To estimate the amount of chemical energy from DZ binding that is transmitted to the pore gate, we employed a simple model of channel gating between closed (C) and open (O) pore states in both unliganded and DZ-bound conditions (*Figure 7A*). The model assumes that gating can be
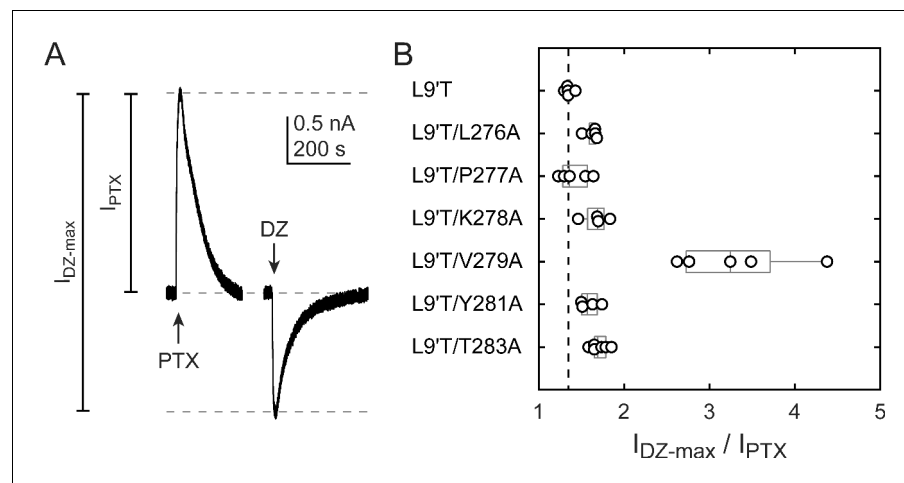

Figure 5. Ratio of maximal DZ-evoked to PTX-sensitive current amplitude. (**A**) Example currents from α_1L9'T/K278A$\beta_2\gamma_{2L}$ receptors elicited by 10 second pulses of either 1 mM PTX or 1 µM DZ. (**B**) Summary of the ratio of maximal DZ-evoked to PTX-sensitive current amplitude for individual oocytes. Gray box plots indicate the median and 25th and 75th percentiles. The vertical dashed line is the mean for L9'T. These ratios were used as estimates for the approximate fold-change in open probability upon DZ binding.
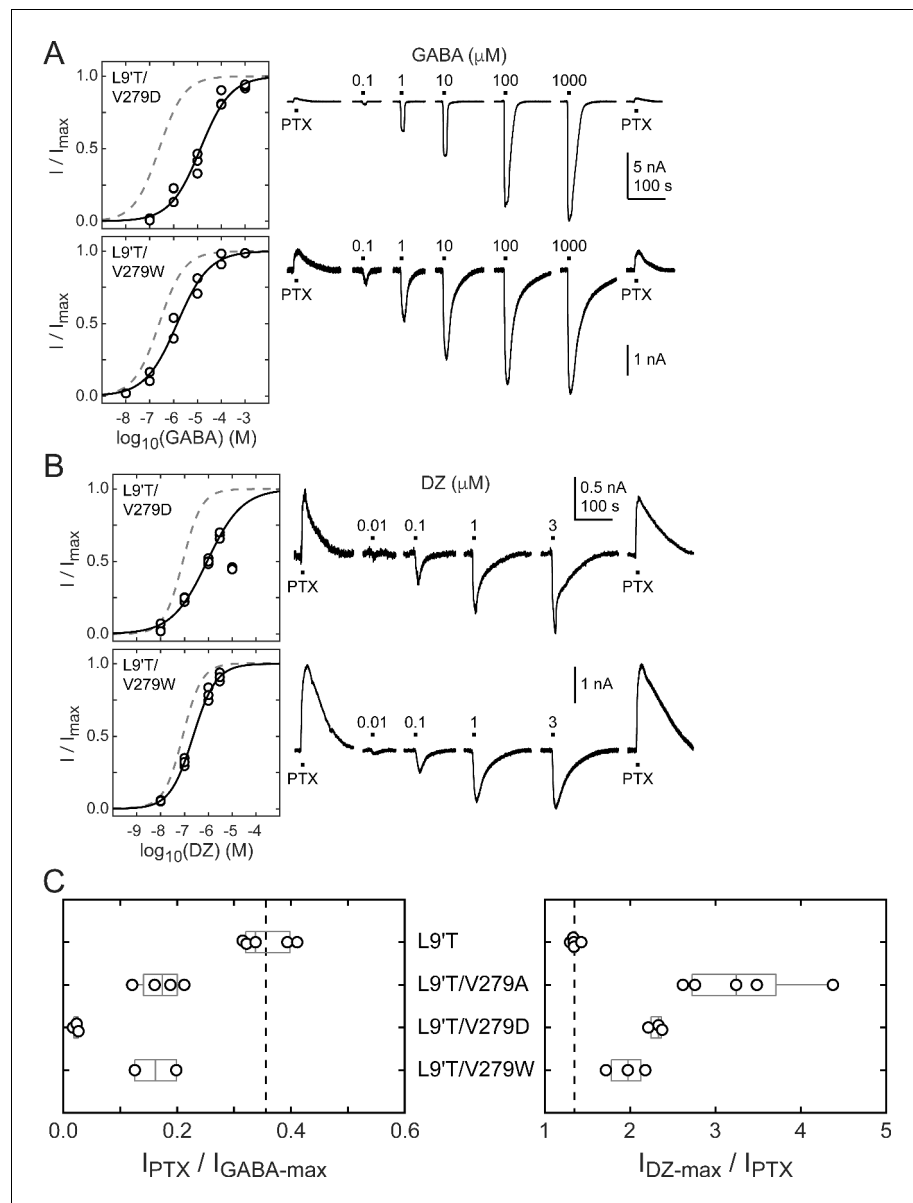
Figure 6. Spontaneous PTX-sensitive and GABA- or DZ-evoked currents for α_1V279D and α_1V279W in the gain of function α_1L9'T$\beta_2\gamma_{2L}$ background. (**A**) Summary of normalized GABA concentration–response relationships for GABA-evoked currents with the zero current baseline set to the level of spontaneous activity (left). Solid line is a fit of the combined data across oocytes to *Equation 1*, and the dashed line is the fit for the L9'T background. Fit parameters are EC$_{50}$, hill slope (# oocytes): L9'T/V279D = 13 µM, 0.68 (3); L9'T/V279W = 1.4 µM, 0.65 (2). Example currents in response to 10 second pulses of the pore blocker PTX (1 mM) or GABA (concentration in micromolar indicated above each pulse) (right). (**B**) Same as in (**A**) except for DZ-evoked currents. Responses from L9'T/V279D to 10 µM DZ were excluded from the fit. Fit parameters are EC$_{50}$, hill slope (# oocytes): L9'T/V279D = 0.88 µM, 0.58 (3); L9'T/V279W = 0.23 µM, 0.90 (3). (**C**) Summary of the ratios of PTX-sensitive and either maximal GABA- or DZ-evoked current amplitudes for individual oocytes. Gray box plots indicate the median and 25th and 75th percentiles. The vertical dashed line is the mean for L9'T. These ratios were used as estimates for the approximate fold-change in open probability upon DZ binding.

approximated with a single closed and open states in each liganded condition. The free energy differences for pore gating in unliganded (ΔG_0) and DZ-bound (ΔG_1) conditions were calculated according to *Equations 2–3* under the assumption that $P_{o\text{-GABA-max}} \sim 1$. A comparison of ΔG_0 versus ΔG_1 shows that DZ binding confers a uniform $\Delta\Delta G_{DZ} = \Delta G_1 - \Delta G_0 = -0.4$ kcal/mol to the pore gating
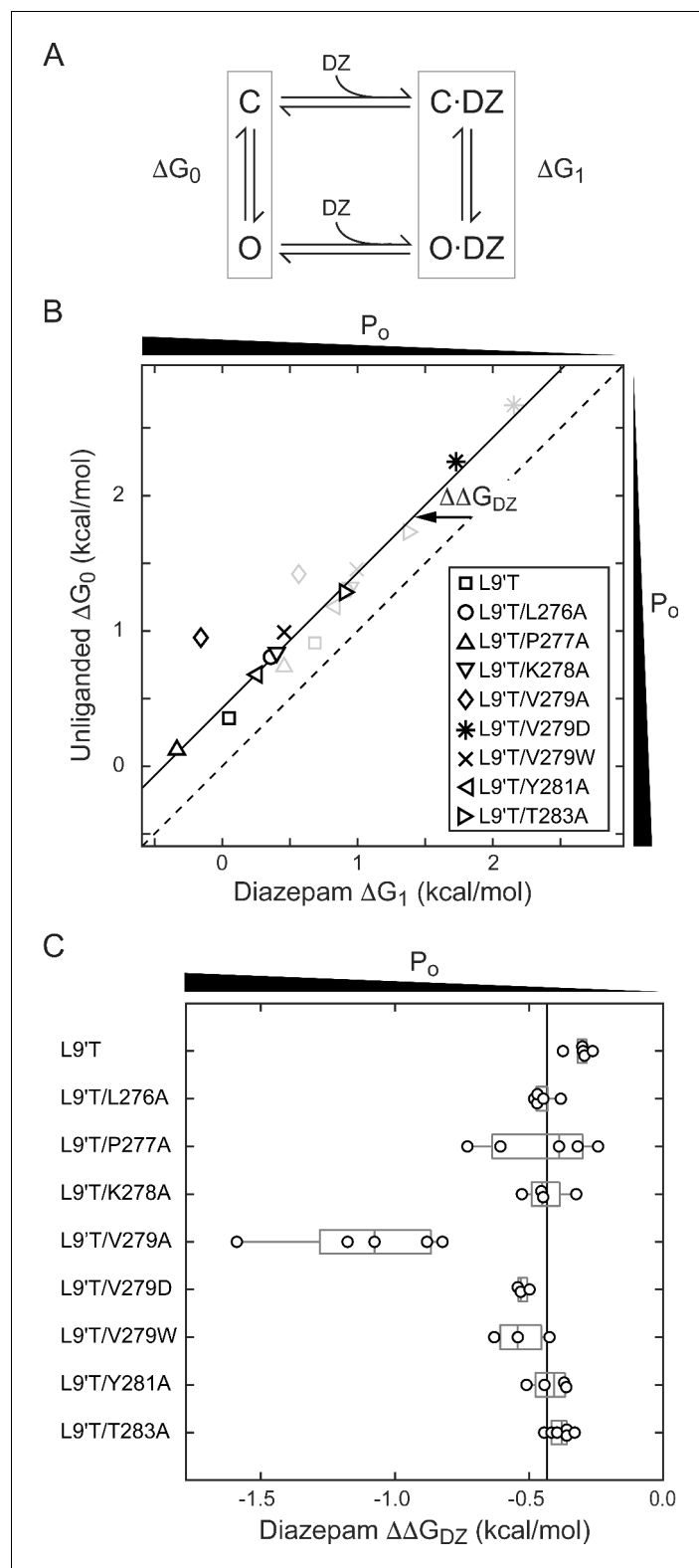
Figure 7. A critical residue in the α_1M2–M3 linker regulating DZ's energetic contribution to pore gating. (**A**) A simple model approximating channel gating between closed (C) and open (O) pore states in both unliganded and DZ-bound conditions. (**B**) Relationship between gating free energy in unliganded (ΔG_0) and DZ-bound (ΔG_1) conditions for α_1L9'T$\beta_2\gamma_{2L}$ receptors and α_1M2–M3 linker mutations assuming $P_{o-GABA-max} = 1$ (bold symbols) or $P_{o-GABA-max} = 0.5$ (light gray symbols) (Equations 2–3). ΔG values are the change in energy from closed to open

Figure 7 continued on next page

Figure 7 continued

states, such that negative values favor opening. To illustrate this, we indicate the direction of increasing open probability (P_o) along each axis. Points are the mean across oocytes. The dashed line of symmetry reflects $\Delta G_0 = \Delta G_1$ where DZ would have no effect on pore gating. The solid line is a fit to $\Delta G_1 = \Delta G_0 + \Delta\Delta G_{DZ}$ for all of the data points except the outlier α_1V279A given $P_{o-GABA-max} = 1$. The good description of the data suggests that DZ's energetic contribution to pore gating is the same for all of the constructs on this line, estimated as $\Delta\Delta G_{DZ} = -0.4$ kcal/mol. In contrast, α_1V279A more than doubles the energy that DZ binding transmits to the pore gate. A comparison of the bold and light gray symbols shows that reducing $P_{o-GABA-max}$ to 0.5 primarily shifts the data points along the fitted line with only minor changes in $\Delta\Delta G_{DZ}$, indicating that our assumption for the value of $P_{o-GABA-max}$ is not critical for interpretation of $\Delta\Delta G_{DZ}$. Nonetheless, we verified that single L9'T/V279A receptors open with high probability (*Figure 7—figure supplement 1*). (C) Summary of $\Delta\Delta G_{DZ}$ for individual oocytes. Negative values of $\Delta\Delta G_{DZ}$ increase channel open probability. Gray box plots indicate the median and 25th and 75th percentiles. The vertical line is the position of linear fit in (B) corresponding to −0.4 kcal/mol.

The online version of this article includes the following figure supplement(s) for figure 7:

Figure supplement 1. Single-channel opening for L9'T/V279A in saturating GABA.

equilibrium independent of α_1M2–M3 linker mutation with the notable exception f α_1V279A that more than doubles $\Delta\Delta G_{DZ}$ (*Figure 7B,C* and *Table 1*). Importantly, this result is largely independent of our assumption for $P_{o-GABA-max}$ (see bold vs. light gray symbols in *Figure 7B*). Nonetheless, we verified that single L9'T/V279A channels in saturating GABA open with high probability to a similar maximal conductance level as wild-type and L9'T channels (*Figure 7—figure supplement 1*). These observations suggest that coupling between the BZD site and pore gate is relatively independent of individual α_1M2–M3 linker side chain interactions except for α_1V279, which natively hinders DZ gating as compared to its substitution with alanine. Strikingly, introduction of a bulky tryptophan or charged aspartate at position 279 have much smaller effects on $\Delta\Delta G_{DZ}$, consistent with the idea that the small side chain volume of alanine is the most relevant factor for increased DZ efficiency.

The mutation α_1V279A enhances DZ potentiation of GABA-evoked currents in a wild-type background

If gating in the α_1L9'T background is relevant to neurotransmitter-driven gating in native receptors, then the mutation α_1V279A should both impair gating by GABA and enhance DZ potentiation of GABA-evoked currents in a wild-type background. To test this, we compared GABA-evoked current responses in $\alpha_1\beta_2\gamma_{2L}$ (wild-type) and α_1V279A$\beta_2\gamma_{2L}$ (V279A) receptors, as well as the ability of 1 μM DZ to potentiate these responses. First, GABA EC$_{50}$ is increased by α_1V279A, consistent with impaired unliganded gating (*Figure 8A*). This effect is similar, although slightly larger than previously observed in $\alpha_2\beta_1\gamma_{2S}$ receptors (*O'Shea and Harrison, 2000*). Second, DZ potentiates GABA-evoked peak current responses to a greater extent in V279A than in wild-type receptors, consistent with enhanced coupling between the BZD site and pore gate in the mutant (*Figure 8B,C*). In contrast to wild-type, DZ also potentiates V279A currents evoked with a saturating concentration of GABA. Together, these data suggest that the additional DZ modulation conferred by α_1V279A is both independent of agonist association and additive to DZ potentiation in wild-type receptors.

In addition to the BZD positive modulator DZ, we examined the effect of the α_1V279A mutation on the BZD negative modulator FG-7142 (*Im et al., 1995*). Responses to ~EC$_{20-25}$ GABA were reduced in the presence of FG-7142 in both WT and V279A receptors, but to a slightly lesser extent in V279A (*Figure 8—figure supplement 1*). Distinct mechanisms for BZD positive and negative modulation could explain the observed reduction in negative modulation as compared to enhancement of positive modulation conferred by α_1V279A. Alternatively, our observations are also consistent with the idea that α_1V279A stabilizes an open channel configuration specifically in the BZD-bound complex and that this stabilization works in concert with positive modulators but hinders negative modulators.

α_1L9'T and α_1V279A have independent and additive effects on the pore-gating equilibrium

To further explore the idea that α_1V279A confers its effects primarily by altering pore gating in DZ-bound receptors, we asked whether a simple Monod–Wyman–Changeux (MWC) model of receptor
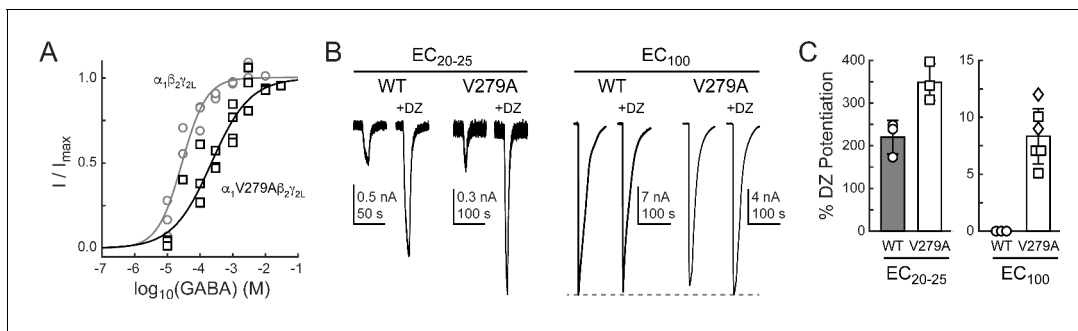
Figure 8. The mutation α_1V279A enhances DZ potentiation of GABA-evoked current amplitudes in a wild-type (WT) $\alpha_1\beta_2\gamma_{2L}$ background. (**A**) Normalized GABA concentration–response relationships for WT (circles, three oocytes) and V279A (squares, four oocytes). Solid lines are fits to *Equation 1* for all oocytes combined. Fit parameters are EC_{50}, hill slope (# oocytes): WT = 28 μM, 1.2 (3); V279A = 222 μM, 0.7 (4). (**B**) Potentiation of current amplitudes evoked by 10 second pulses of either subsaturating EC_{20-25} (WT: 10 μM, V279A: 30 μM) or saturating EC_{100} (WT: 3 mM, V279A: 3–30 mM) GABA by 1 μM DZ. (**C**) Summary of potentiation as shown in (**B**) for individual oocytes. For V279A EC_{100}, squares indicate 3 or 10 mM GABA and diamonds 30 mM GABA.

The online version of this article includes the following figure supplement(s) for figure 8:

Figure supplement 1. Reduction of GABA-evoked currents by the BZD negative modulator FG-7142 for $\alpha_1\beta_2\gamma_{2L}$ (WT) and α_1V279A$\beta_2\gamma_{2L}$ (V279A) receptors.

behavior can account for our observations (*Figure 9A*). This model has been widely used to describe pseudo-steady-state behavior in GABA$_A$ receptors (*Steinbach and Akk, 2019*; *Rüsch and Forman, 2005*; *Chang and Weiss, 1999*). For comparison with model simulations, we estimated open probability (P_o) as a function of GABA or DZ concentration (black curves in *Figure 9B*) from fits of *Equation 1* to the data shown in *Figures 2*, *4*, and *8* where the minimum and maximum P_o were scaled according to our observed PTX-sensitive and GABA- or DZ-evoked current amplitudes. In the α_1L9'T background, the maximum GABA-evoked P_o was allowed to vary during optimization, and the minimum unliganded P_o was scaled relative to the maximum by the observed mean ratio of $I_{PTX}/I_{GABA\text{-}max}$ (*Figure 3*). The maximum DZ-evoked P_o was scaled relative to the minimum unliganded P_o by the observed mean ratio of $I_{DZ\text{-}max}/I_{PTX}$ (*Figure 5*). The maximal P_o was set to 0.85 for $\alpha_1\beta_2\gamma_{2L}$ receptors (*Keramidas and Harrison, 2010*) and allowed to vary for α_1V279A$\beta_2\gamma_{2L}$ receptors.

The model assumes independent GABA and DZ binding. Model parameters were optimized by globally minimizing the sum of squared residuals between simulated (*Equation 4*) and estimated P_o as a function of GABA or DZ concentration for α_1L9'T$\beta_2\gamma_{2L}$, α_1L9'T/V279A$\beta_2\gamma_{2L}$, and $\alpha_1\beta_2\gamma_{2L}$ receptors (*Figure 9B*). Responses to α_1V279A$\beta_2\gamma_{2L}$ receptors were not considered during optimization and treated as a model prediction. The mutations α_1L9'T and α_1V279A were allowed to perturb the parameter L with the assumption that their effects are independent in the L9'T/V279A double mutant. For wild-type receptors, L was fixed according to its approximate relation with EC_{50} as $L_{WT} = L_{L9T}\left(EC_{50,WT}/EC_{50,L9T}\right)^2$ (*Steinbach and Akk, 2019*; *Akk et al., 2018*; *Scheller and Forman, 2002*; *Chang and Weiss, 1999*). The value of d was assumed to be the same for L9'T and wild-type receptors and allowed to vary in the presence of the α_1V279A mutation. The resulting optimized model parameters (*Figure 9* caption) were highly constrained by the data (i.e. estimated P_o), and the model does a fairly good job of describing our observed responses to either GABA or DZ, differing somewhat in the steepness of their concentration dependence (*Figure 9B*). Furthermore, the model qualitatively accounts for observations from α_1V279A$\beta_2\gamma_{2L}$ receptors even though they were not considered during optimization. The model's predicted maximum P_o approached 1.0 in the α_1L9'T background, consistent with a gain of function phenotype. In contrast, maximal P_o was reduced in α_1V279A$\beta_2\gamma_{2L}$ as compared to wild-type receptors, as expected for a reduction in unliganded activity. These results suggest that α_1L9'T and α_1V279A have independent and additive effects on the gating equilibrium, and that for α_1V279A, this effect depends on DZ occupancy.

Although responses to GABA or DZ alone are largely explained by this model, DZ potentiation of GABA-evoked responses in a wild-type background is either underestimated or overestimated for subsaturating or saturating GABA concentrations, respectively (*Figure 9C*). Previous applications of
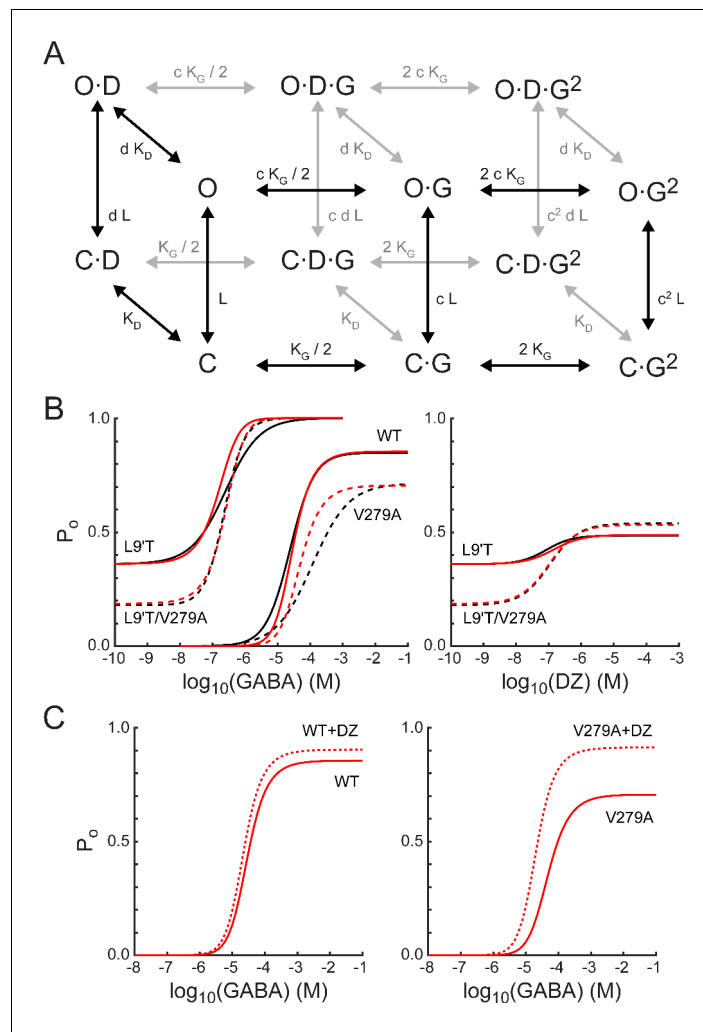
Figure 9. A simple MWC model of channel gating largely accounts for the observed effects of α_1L9′T and α_1V279A via independent and additive effects on the pore-gating equilibrium. (**A**) The model depicts channel gating between closed (C) and open (O) states with independent binding of two GABA (G) and one DZ (D) molecule. L is the ratio of closed to open state probabilities in the absence of ligand, K_G and K_D are the respective dissociation constants for GABA or DZ, and c and d are the respective factors by which GABA or DZ binding influence channel opening. The probability to be in an open state is given by *Equation 4*. (**B**) Estimated open probability (P_o) from the data in *Figures 2–5* (black) overlaid with model simulations (*Equation 4*, red). See main text for a detailed description. Model parameters are: $L_{L9′T}$ = 1.8; $L_{L9′T/V279A}$ = 4.4; L_{WT} = 18000; K_G = 53 μM; K_D = 180 nM; c = 0.0031; d = 0.59; d_{V279A} = 0.20. (**C**) The model's prediction for potentiation of WT and V279A GABA-evoked responses by 1μM DZ.

The online version of this article includes the following source data and figure supplement(s) for figure 9:

Source code 1. MWC simulation code.

Figure supplement 1. Estimated open probability (P_o) from the data in *Figure 2* (black) overlaid with simulations for the model in *Figure 9A* (red).

this model to BZD modulation in gain of function backgrounds predict a larger left shift of the P_o curve in the presence of drug more similar to that observed, in part due to a smaller value of d (*Campo-Soria et al., 2006*; *Downing et al., 2005*; *Rüsch and Forman, 2005*). However, reducing d also enhances the predicted potentiation of responses to saturating GABA, contrary to that observed for wild-type receptors. Thus, the model is either too simplistic or its assumptions too strict to describe all aspects of DZ potentiation in wild-type channels that both rapidly desensitize and may involve drug modulation of agonist binding and/or intermediate gating steps (*Goldschen-*

Ohm et al., 2014; *Gielen et al., 2012*). Nonetheless, the model does predict an increase in DZ potentiation of responses evoked by both subsaturating and saturating GABA for α_1V279A, qualitatively similar to that observed. For responses to saturating GABA in V279A, 42% of the predicted potentiation is accounted for by the lower $P_{o\text{-GABA-max}}$ as compared to WT, and the remainder reflects the mutations enhancement of DZ gating.

Effects of alanine mutations on gating by GABA

To explore the effects of the mutations on gating by GABA, we fit estimated open probability versus GABA concentration relationships using the model in *Figure 9A* (front face only in the absence of DZ). Estimated open probabilities from fits of *Equation 1* to the data in *Figure 2* were scaled according to the assumption that $P_{o\text{-GABA-max}} = 1$ as described above. We first asked whether all of the mutations could be explained solely by differences in their intrinsic closed–open equilibrium (parameter L). *Figure 9—figure supplement 1A* shows model predictions where all constructs share identical affinities for GABA (i.e. parameters K_G and c). The overall rough qualitative agreement with the data suggests that differences in unliganded open probability are likely to account for much of the observed effects. For comparison, we next constrained L based on the estimated unliganded P_o as $L = (1 - P_o)/P_o$ and allowed GABA affinity to differ across constructs. The resulting model fits were slightly improved to a nearly equivalent extent regardless of whether the relative affinity for closed versus open states (parameter c) was held constant (*Figure 9—figure supplement 1B*) or allowed to vary (*Figure 9—figure supplement 1C*). Thus, the simplest conclusion is that mutations with right-shifted EC_{50}s reduce GABA affinity for the closed state, although we cannot rule out compensatory changes in affinity for closed and open states.

Discussion

The main conclusions of this study are as follows: First, in the α_1L9'T gain of function background alanine substitutions in the α_1M2–M3 linker generally impair unliganded pore opening, indicating that side chain interactions with the linker are important for gating even in the absence of bound agonist. Second, the same mutations have no effect on the amount of chemical energy from DZ binding transmitted to the pore gate, except for α_1V279A which more than doubles DZ's energetic contribution to pore gating. Thus, α_1V279 plays a crucial role to natively hinder drug modulation as compared to its substitution with alanine. Third, introduction of a bulky tryptophan or charged aspartate at position 279 is less favorable than the smaller alanine, suggesting that DZ modulation is inhibited by side chain interactions at the center of the linker. Fourth, α_1V279D severely impairs unliganded gating. Fifth, α_1V279A similarly enhances DZ potentiation of GABA-evoked currents in a wild-type background. Sixth, the effects of α_1V279A in both α_1L9'T and wild-type backgrounds are explained by specific changes in the pore gating equilibrium and its coupling to DZ binding at the BZD site.

The use of gain of function mutations to study modulatory or weakly activating ligands is well appreciated (*Germann et al., 2019*; *Akk et al., 2018*; *Campo-Soria et al., 2006*; *Downing et al., 2005*; *Rüsch and Forman, 2005*; *Findlay et al., 2001*). Single-channel gating dynamics for combinations of gain of function mutations in AChR suggest that the unliganded and agonist-bound gating mechanisms are similar if not identical and also that they are similarly affected by mutations (*Purohit and Auerbach, 2009*). Consistent with this idea, MWC models of pseudo steady-state GABA$_A$R function have been largely successful in describing the effects of gain of function mutations with changes to the pore gating equilibrium independent of agonist binding (*Steinbach and Akk, 2019*; *Downing et al., 2005*; *Campo-Soria et al., 2006*; *Rüsch and Forman, 2005*; *Chang and Weiss, 1999*). The model reported here in *Figure 9* supports this conclusion.

Although the effects of α_1V279A can also be explained by specific changes to the pore-gating equilibrium, they are dependent on DZ occupation of the BZD site. From the model in *Figure 9A*, we compute an efficiency for GABA of $\eta_{GABA} = [1 - log(K_G)/log(cK_G)] \times 100\% = 37\%$, similar to that reported previously (*Nayak et al., 2019*). In contrast, DZ efficiency is $\eta_{DZ} = [1 - log(K_D)/log(dK_D)] \times 100\% = 3\%$. Whereas α_1V279A decreases unliganded pore opening, it also increases DZ efficiency ($\eta_{DZ,V279A} = 9\%$) to the extent that DZ binding overcomes its intrinsic inhibitory effect and results in similar or even enhanced activation as compared to wild type (*Figure 9*). Interestingly, an M2–M3 linker mutation in the γ_2 subunit was similarly observed to impair

activation by GABA and enhance modulation by the general anesthetic propofol (*O'Shea et al., 2009*).

Our estimates for the energetic effect of DZ binding on pore gating (−0.4 kcal/mol) are similar to prior estimates from direct gating in L9'S/T backgrounds and from kinetic models (*Goldschen-Ohm et al., 2014*; *Gielen et al., 2012*; *Downing et al., 2005*; *Rüsch and Forman, 2005*). This is approximately 10-fold less than the energy derived from binding each molecule of GABA (*Goldschen-Ohm et al., 2014*; *Maksay, 1994*; *Jackson, 1992*). However, it is sufficient to produce a relevant change in open probability in channels with small free energy differences between closed and open states, such as conferred by single bound agonists, partial agonists, other allosteric modulators, or gain of function mutations. From a clinical perspective, such small perturbations are likely to be more easily tolerated in patients. Given that the M2–M3 linker is associated with early movements during AChR activation (*Purohit et al., 2013*), it is possible that biasing the linker toward its active conformation in the α_1L9'T background could limit our ability to observe its full range of motion. In this case, our observed effects of linker mutations on DZ modulation may underestimate their effects on the full activation pathway.

The interface between the extracellular agonist- and BZD-binding domains and the transmembrane helices is formed largely by several loops including the M2–M3 linker, Cys loop, β1–β2 loop and β8–β9 linker, and pre-M1 segment from neighboring subunits (*Figure 1*). Mutagenesis suggests that interactions between these domains are important for channel gating by agonists (*Kash et al., 2003*; *O'Shea and Harrison, 2000*) thought to involve an outward radial displacement of the M2–M3 linker (*Nemecz et al., 2016*). Rate versus free energy linear relationships in AChR suggest that the M2–M3 linker moves early during channel activation, similar to rearrangements at agonist binding sites (*Purohit et al., 2013*). Consistent with these observations, mutant cycle analysis indicates strong long-range coupling between residues in the M2–M3 linker and agonist binding sites (*Gupta et al., 2017*). Given the homology between the BZD site at the α/γ interface and agonist sites at β/α interfaces, interactions between the M2–M3 linker and BZD site are reasonable, although they need not be very strong given the relatively small energy DZ contributes to pore gating. As with agonist sites, such interactions could be mediated by global backbone conformational fluctuations or via distinct structural components, or both. Either way, side chain interactions at position 279 in the α_1 subunit play an important role in coupling between the BZD site and pore gate.

In structural models, the M2–M3 linker adopts a C-shaped conformation with α_1V279 oriented inwards toward the center of the arc (*Figure 1D*; *Kim et al., 2020*; *Laverty et al., 2019*; *Masiulis et al., 2019*; *Phulera et al., 2018*; *Zhu et al., 2018*). We hypothesize that the side chain at position 279 is centrally involved in steric interactions between linker residues near the top of the M2 and M3 helices. Removing this obstruction (α_1V279A) would allow the linker to become more compact and bring the M2 and M3 helices closer together. In contrast, similar or larger side chains (α_1V279D/W) would sterically inhibit such a conformational change. In this case, we speculate that the closer proximity of the M3 helix could impair unliganded pore gating by hindering radial expansion of the pore lining M2 helix. Conversely, a more compact transmembrane domain may also enhance coupling with the BZD site (*Kim et al., 2020*). Valine and threonine residues in GlyR and AchR aligning with V279 (*Figure 1—figure supplement 1*) adopt a similar conformation (*Kumar et al., 2020*; *Nemecz et al., 2016*; *Du et al., 2015*), suggesting that this residue has a conserved role in other pLGICs.

Alternatively, removing most of the central side chain may simply alter linker flexibility. Linker flexibility has been suggested to be inversely correlated with gating, where stabilizing interactions between α_1R19' (located just below α_1V279) and the linker backbone may promote coupling between extracellular and intracellular domains (*Masiulis et al., 2019*). Thus, the strong inhibition of unliganded opening conferred by α_1V279D could reflect competition for α_1R19', thereby weakening its interaction with the linker backbone and increasing linker flexibility. However, this does not provide a simple explanation for the opposing effects of α_1V279A on unliganded versus DZ-bound gating. Regardless, it is important to keep in mind that the energetic changes that we observe for DZ gating are on the order of a hydrogen bond or two, and thus can be accounted for by relatively subtle changes.

The β8-β9 linker and pre-M1 in the neighboring γ_2 subunit come in close proximity to the α_1M2–M3 linker and are known to be important for BZD modulation, with the β8-β9 linker also contributing to the BZD-binding site (*Hanson and Czajkowski, 2011*; *Hanson and Czajkowski, 2008*). In AChR

strong coupling with the adjacent β8-β9 linker and pre-M1 segment of the neighboring subunit occurs primarily via the threonine aligning with α_1V279 in GABA$_A$R and its neighboring serine (*Gupta et al., 2017*). A reorientation of the linker due to removal of steric interactions near its center could alter coupling to the BZD site via interactions with the γ_2 β8-β9 linker and/or pre-M1. For example, a compression of the ends of the M2–M3 linker would cause the middle of the linker to be squeezed outward toward the neighboring γ_2 subunit, potentially enhancing intersubunit coupling. Comparison of GlyR structures in apo or antagonist-bound versus agonist-bound conformations indicates that intersubunit interactions between the M2–M3 linker in the vicinity of the valine aligning with V279 and the following serine, and the top of the M1 helix in the adjacent subunit are weakened during channel activation (*Du et al., 2015*; *Kumar et al., 2020*). Thus, a stronger intersubunit coupling in this area could potentially both reduce unliganded opening and enhance coupling with rearrangements of the γ_2 subunit upon BZD binding. However, other regions including the β4-β5 linker in the channel's outer vestibule also affect BZD modulation of agonist-evoked currents (*Pflanz et al., 2018*; *Venkatachalan and Czajkowski, 2012*). Thus, BZD modulation likely involves larger domain fluctuations in addition to any specific molecular pathways involving α_1V279.

Recent structures of αβγ receptors show DZ bound not only at the classical α/γ site in the extracellular domain, but also in the transmembrane domain below the M2–M3 linker at β/α and γ/β intersubunit interfaces (*Kim et al., 2020*; *Masiulis et al., 2019*). Thus, it is intriguing to speculate that enhanced DZ gating as conferred by α_1V279A may involve occupation of a transmembrane site. However, these structures were solved in the presence of 100–200 μM DZ, and the relevance of these transmembrane sites to high affinity binding of ~1 μM DZ at the classical site is unclear (*Walters et al., 2000*). Also, DZ binding in the transmembrane domain was not observed at α/γ or α/β interfaces. Therefore, we favor the interpretation that our observed effects reflect altered functional coupling with the classical site.

Our observations reveal a critical residue V279 in the α_1M2–M3 linker, which regulates energetic coupling between the BZD site and the pore gate, whereas other linker side chains contribute little or not at all. These data shed new light on the molecular basis for GABA$_A$R modulation by one of the most widely prescribed classes of psychotropic drugs.

Materials and methods

Mutagenesis and expression in oocytes

DNA for wild-type GABA$_A$R rat α_1, β_2, and γ_{2L} subunits were a gift from Dr. Cynthia Czajkowski. Single alanine substitutions were introduced throughout the α_1M2–M3 linker from L276-T283 in addition to the gain of function α_1L9'T pore mutation (rat α_1L263T) (QuikChange II, Qiagen). Mutations V279D and V279W were introduced similarly. Each construct was verified by forward and reverse sequencing of the entire gene. mRNA for each construct was generated (mMessage mMachine T7, Ambion) for expression in *X. laevis* oocytes (EcoCyte Bioscience, Austin, TX). Oocytes were injected with 27–54 ng of total mRNA for α, β, and γ subunits in a 1:1:10 ratio (*Boileau et al., 2002*) (Nanoject, Drummond Scientific). Oocytes were incubated in ND96 (in mM: 96 NaCl, 2 KCl, 1 MgCl$_2$, 1.8 CaCl$_2$, 5 HEPES, pH 7.2) with 100 mg/ml gentamicin at 18°C.

Two-electrode voltage clamp recording and analysis

Currents from expressed channels 1–3 days post-injection were recorded in two-electrode voltage clamp (Dagan TEV-200, HEKA ITC and Patchmaster software). Oocytes were held at −80 mV and perfused continuously with buffer (ND96) or buffer containing PTX, GABA, or DZ. PTX was diluted from a 1 M stock solution in DMSO. DZ was diluted from a 10 mM stock solution in DMSO. Fresh PTX and DZ stock solutions were tested several times with no change in results. GABA was dissolved directly from powder. A microfluidic pump (Elveflow OB1 MK3+) and rotary valve (Elveflow MUX Distributor) provided consistent and repeatable perfusion and solution exchange across experiments, which limited solution exchange variability to primarily differences between oocytes only. Ten second pulses of PTX, GABA, or DZ were followed by 3–6 min in buffer to allow currents to return to baseline. Recorded currents were analyzed with custom scripts in MATLAB (Mathworks). Recordings of concentration–response relationships were bookended by pulses of PTX to correct for any drift or rundown during the experiment. Briefly, currents were baseline subtracted to correct for

drift and then scaled by a linear fit to the peak of each PTX response to correct for rundown (*Figure 2—figure supplement 1*). The amount of current rundown was variable across oocytes, with no clear relation to specific constructs. Concentration–response relationships were fit to the Hill equation:

$$\frac{I}{I_{max}} = \frac{1}{1 + \left(\frac{EC_{50}}{[X]}\right)^n} \tag{1}$$

where I is the peak current response, $[X]$ is ligand concentration, EC_{50} is the concentration eliciting a half-maximal response, and n is the Hill slope.

Single-channel recording

HEK293T cells were transfected with DNA for rat α_1L9'T/V279A, β_2 and γ_{2L} subunits in a 1:1:1 ratio. Single-channel currents were recorded 16–32 hr post-transfection from excised inside-out patches clamped at −80 mV. Currents were acquired at 20 kHz and low-pass filtered at 2 kHz (Axopatch 200A, HEKA ITC, and PatchMaster software). Extracellular (pipet) solution was (in mM): 145 NaCl, 2.5 KCl, 2 CaCl$_2$, 1 MgCl$_2$, 10 HEPES, 4 Dextrose, pH 7.3 with NaOH. Intracellular (bath) solution was (in mM): 140 KCl, 10 EGTA, 10 HEPES, 2 MgATP, pH 7.3 with KOH. GABA was dissolved in the extracellular solution.

DZ-gating model

For the model in *Figure 7A*, the free energy difference for unliganded (ΔG_0) and DZ-bound (ΔG_1) gating was estimated as follows:

$$\Delta G_0 = -kT\,ln\left(\frac{P_{open}}{P_{closed}}\right)_{unliganded} \approx -kT\,ln\left(\frac{P_{o-GABA-max}(I_{PTX}/I_{GABA-max})}{1 - P_{o-GABA-max}(I_{PTX}/I_{GABA-max})}\right) \tag{2}$$

$$\Delta G_1 = -kT\,ln\left(\frac{P_{open}}{P_{closed}}\right)_{DZ-bound} \approx -kT\,ln\left(\frac{P_{o-GABA-max}(I_{DZ-max}/I_{GABA-max})}{1 - P_{o-GABA-max}(I_{DZ-max}/I_{GABA-max})}\right) \tag{3}$$

where I_{PTX}, $I_{GABA-max}$, and I_{DZ-max} are as shown in *Figures 3* and *5*, k is the Boltzmann constant, T is temperature, and $P_{o-GABA-max}$ is the open probability in saturating GABA, which was assumed to be approximately 1. Importantly, even if this assumption is incorrect, the effect on DZ's energetic contribution to pore gating should be minimal and our overall conclusion unchanged (see *Figure 7B*). Also, this assumption was verified for single L9'T/V279A receptors (*Figure 7—figure supplement 1*).

MWC model

For the model in *Figure 9A*, the probability to be in an open (O) state is given by:

$$P_o = \left(1 + L\frac{\left(1 + \frac{[DZ]}{K_D}\right)\left(1 + \frac{[GABA]}{K_G}\right)^2}{\left(1 + \frac{[DZ]}{dK_D}\right)\left(1 + \frac{[GABA]}{cK_G}\right)^2}\right)^{-1} \tag{4}$$

where L is the ratio of closed (C) to open (O) state probabilities in the absence of ligand, K_G and K_D are the respective dissociation constants for GABA or DZ, and c and d are the respective factors by which GABA or DZ binding influence pore opening.

Additional information

Author contributions

Joseph W Nors, Data curation, Software, Formal analysis, Validation, Investigation, Visualization, Writing - original draft, Writing - review and editing; Shipra Gupta, Resources, Investigation; Marcel P Goldschen-Ohm, Conceptualization, Data curation, Software, Formal analysis, Supervision, Visualization, Methodology, Project administration, Writing - review and editing

Author ORCIDs

Marcel P Goldschen-Ohm ID https://orcid.org/0000-0003-1466-9808

Decision letter and Author response

Decision letter https://doi.org/10.7554/eLife.64400.sa1
Author response https://doi.org/10.7554/eLife.64400.sa2

Additional files

Supplementary files

• Transparent reporting form

Data availability

Source code for the modeling depicted in Figure 9 has been provided.

References

Agarwal SD, Landon BE. 2019. Patterns in outpatient benzodiazepine prescribing in the United States. *JAMA Network Open* **2**:e187399. DOI: https://doi.org/10.1001/jamanetworkopen.2018.7399, PMID: 30681713

Akk G, Shin DJ, Germann AL, Steinbach JH. 2018. GABA type A receptor activation in the allosteric coagonist model framework: relationship between EC_{50} and basal activity. *Molecular Pharmacology* **93**:90–100. DOI: https://doi.org/10.1124/mol.117.110569, PMID: 29150461

Bachhuber MA, Hennessy S, Cunningham CO, Starrels JL. 2016. Increasing benzodiazepine prescriptions and overdose mortality in the United States, 1996-2013. *American Journal of Public Health* **106**:686–688. DOI: https://doi.org/10.2105/AJPH.2016.303061, PMID: 26890165

Bode A, Lynch JW. 2014. The impact of human hyperekplexia mutations on glycine receptor structure and function. *Molecular Brain* **7**:2. DOI: https://doi.org/10.1186/1756-6606-7-2, PMID: 24405574

Boileau AJ, Baur R, Sharkey LM, Sigel E, Czajkowski C. 2002. The relative amount of cRNA coding for gamma2 subunits affects stimulation by benzodiazepines in GABA(A) receptors expressed in *Xenopus* oocytes. *Neuropharmacology* **43**:695–700. DOI: https://doi.org/10.1016/S0028-3908(02)00036-9, PMID: 12367615

Braat S, Kooy RF. 2015. The GABAA receptor as a therapeutic target for neurodevelopmental disorders. *Neuron* **86**:1119–1130. DOI: https://doi.org/10.1016/j.neuron.2015.03.042, PMID: 26050032

Campo-Soria C, Chang Y, Weiss DS. 2006. Mechanism of action of benzodiazepines on $GABA_A$ receptors. *British Journal of Pharmacology* **148**:984–990. DOI: https://doi.org/10.1038/sj.bjp.0706796, PMID: 16783415

Chang Y, Weiss DS. 1999. Allosteric activation mechanism of the alpha 1 beta 2 gamma 2 gamma-aminobutyric acid type A receptor revealed by mutation of the conserved M2 leucine. *Biophysical Journal* **77**:2542–2551. DOI: https://doi.org/10.1016/S0006-3495(99)77089-X, PMID: 10545355

Chowdhury S, Chanda B. 2013. Free-energy relationships in ion channels activated by voltage and ligand. *Journal of General Physiology* **141**:11–28. DOI: https://doi.org/10.1085/jgp.201210860

Colquhoun D. 1998. Binding, gating, affinity and efficacy: the interpretation of structure-activity relationships for agonists and of the effects of mutating receptors. *British Journal of Pharmacology* **125**:923–947. DOI: https://doi.org/10.1038/sj.bjp.0702164

Connolly CN, Wafford KA. 2004. The Cys-loop superfamily of ligand-gated ion channels: the impact of receptor structure on function. *Biochemical Society Transactions* **32**:529–534. DOI: https://doi.org/10.1042/bst0320529

Downing SS, Lee YT, Farb DH, Gibbs TT. 2005. Benzodiazepine modulation of partial agonist efficacy and spontaneously active GABA(A) receptors supports an allosteric model of modulation. *British Journal of Pharmacology* **145**:894–906. DOI: https://doi.org/10.1038/sj.bjp.0706251, PMID: 15912137

Du J, Lü W, Wu S, Cheng Y, Gouaux E. 2015. Glycine receptor mechanism elucidated by electron cryo-microscopy. *Nature* **526**:224–229. DOI: https://doi.org/10.1038/nature14853

Findlay GS, Ueno S, Harrison NL, Harris RA. 2001. Allosteric modulation in spontaneously active mutant γ-aminobutyric acidA receptors. *Neuroscience Letters* **305**:77–80. DOI: https://doi.org/10.1016/S0304-3940(01)01646-9

Fluyau D, Revadigar N, Manobianco BE. 2018. Challenges of the pharmacological management of benzodiazepine withdrawal, dependence, and discontinuation. *Therapeutic Advances in Psychopharmacology* **8**:147–168. DOI: https://doi.org/10.1177/2045125317753340, PMID: 29713452

Gao F, Qi L, Yang Z, Yang T, Zhang Y, Xu H, Zhao H. 2018. Impaired GABA neural circuits are critical for fragile X syndrome. *Neural Plasticity* **2018**:1–7. DOI: https://doi.org/10.1155/2018/8423420

Germann AL, Steinbach JH, Akk G. 2019. Application of the co-agonist concerted transition model to analysis of GABAA receptor properties. *Current Neuropharmacology* **17**:843–851. DOI: https://doi.org/10.2174/1570159X17666181206092418, PMID: 30520374

Gibbs TT, Chan CY, Czajkowski CM, Farb DH. 1985. Benzodiazepine receptor photoaffinity labeling: correlation of function with binding. *European Journal of Pharmacology* **110**:171–180. DOI: https://doi.org/10.1016/0014-2999(85)90209-2, PMID: 2985408

Gielen MC, Lumb MJ, Smart TG. 2012. Benzodiazepines modulate GABAA receptors by regulating the preactivation step after GABA binding. *Journal of Neuroscience* **32**:5707–5715. DOI: https://doi.org/10.1523/JNEUROSCI.5663-11.2012

Goldschen-Ohm MP, Wagner DA, Petrou S, Jones MV. 2010. An epilepsy-related region in the GABA(A) receptor mediates long-distance effects on GABA and benzodiazepine binding sites. *Molecular Pharmacology* **77**:35–45. DOI: https://doi.org/10.1124/mol.109.058289, PMID: 19846749

Goldschen-Ohm MP, Haroldson A, Jones MV, Pearce RA. 2014. A nonequilibrium binary elements-based kinetic model for benzodiazepine regulation of GABAA receptors. *Journal of General Physiology* **144**:27–39. DOI: https://doi.org/10.1085/jgp.201411183

Gupta S, Chakraborty S, Vij R, Auerbach A. 2017. A mechanism for acetylcholine receptor gating based on structure, coupling, phi, and flip. *Journal of General Physiology* **149**:85–103. DOI: https://doi.org/10.1085/jgp.201611673

Hales TG, Deeb TZ, Tang H, Bollan KA, King DP, Johnson SJ, Connolly CN. 2006. An asymmetric contribution to γ-Aminobutyric type A receptor function of a conserved lysine within TM2–3 of α1, β2, and γ2 subunits. *Journal of Biological Chemistry* **281**:17034–17043. DOI: https://doi.org/10.1074/jbc.M603599200

Hanson SM, Czajkowski C. 2008. Structural mechanisms underlying benzodiazepine modulation of the GABAA receptor. *Journal of Neuroscience* **28**:3490–3499. DOI: https://doi.org/10.1523/JNEUROSCI.5727-07.2008

Hanson SM, Czajkowski C. 2011. Disulphide trapping of the GABAA receptor reveals the importance of the coupling interface in the action of benzodiazepines. *British Journal of Pharmacology* **162**:673–687. DOI: https://doi.org/10.1111/j.1476-5381.2010.01073.x

Hernandez CC, Macdonald RL. 2019. A structural look at GABAA receptor mutations linked to epilepsy syndromes. *Brain Research* **1714**:234–247. DOI: https://doi.org/10.1016/j.brainres.2019.03.004, PMID: 30851244

Im HK, Im WB, Carter DB, McKinley DD. 1995. Interaction of β-carboline inverse agonists for the benzodiazepine site with another site on GABAA receptors. *British Journal of Pharmacology* **114**:1040–1044. DOI: https://doi.org/10.1111/j.1476-5381.1995.tb13310.x, PMID: 7780638

Jackson MB. 1992. *Thermodynamics of Membrane Receptors and Channels*. CRC Press.

Jones CM, Paulozzi LJ, Mack KA. 2010. Alcohol involvement in opioid pain reliever and benzodiazepine drug abuse-related emergency department visits and drug-related deaths - United states. *MMWR. Morbidity and Mortality Weekly Report* **63**:881–885.

Jones CM, McAninch JK. 2015. Emergency department visits and overdose deaths from combined use of opioids and benzodiazepines. *American Journal of Preventive Medicine* **49**:493–501. DOI: https://doi.org/10.1016/j.amepre.2015.03.040, PMID: 26143953

Kash TL, Jenkins A, Kelley JC, Trudell JR, Harrison NL. 2003. Coupling of agonist binding to channel gating in the GABAA receptor. *Nature* **421**:272–275. DOI: https://doi.org/10.1038/nature01280

Keramidas A, Harrison NL. 2010. The activation mechanism of $\alpha_1\beta_2\gamma_{2S}$ and $\alpha_3\beta_3\gamma_{2S}$ GABAA receptors. *Journal of General Physiology* **135**:59–75. DOI: https://doi.org/10.1085/jgp.200910317

Kim JJ, Gharpure A, Teng J, Zhuang Y, Howard RJ, Zhu S, Noviello CM, Walsh RM, Lindahl E, Hibbs RE. 2020. Shared structural mechanisms of general anaesthetics and benzodiazepines. *Nature* **585**:303–308. DOI: https://doi.org/10.1038/s41586-020-2654-5

Kucken AM, Wagner DA, Ward PR, Teissére JA, Boileau AJ, Czajkowski C. 2000. Identification of benzodiazepine binding site residues in the gamma2 subunit of the gamma-aminobutyric acid(A) receptor. *Molecular Pharmacology* **57**:932–939. PMID: 10779376

Kumar A, Basak S, Rao S, Gicheru Y, Mayer ML, Sansom MSP, Chakrapani S. 2020. Mechanisms of activation and desensitization of full-length glycine receptor in lipid nanodiscs. *Nature Communications* **11**:3752. DOI: https://doi.org/10.1038/s41467-020-17364-5

Laverty D, Desai R, Uchański T, Masiulis S, Stec WJ, Malinauskas T, Zivanov J, Pardon E, Steyaert J, Miller KW, Aricescu AR. 2019. Cryo-EM structure of the human α1β3γ2 GABA_A receptor in a lipid bilayer. *Nature* **565**: 516–520. DOI: https://doi.org/10.1038/s41586-018-0833-4, PMID: 30602789

Li P, Eaton MM, Steinbach JH, Akk G. 2013. The benzodiazepine diazepam potentiates responses of α1β2γ2L γ-aminobutyric acid type A receptors activated by either γ-aminobutyric acid or allosteric agonists. *Anesthesiology* **118**:1417–1425. DOI: https://doi.org/10.1097/ALN.0b013e318289bcd3, PMID: 23407108

Limon A, Reyes-Ruiz JM, Miledi R. 2012. Loss of functional GABA(A) receptors in the alzheimer diseased brain. *PNAS* **109**:10071–10076. DOI: https://doi.org/10.1073/pnas.1204606109, PMID: 22691495

Mahdavi M, Kheirollahi M, Riahi R, Khorvash F, Khorrami M, Mirsafaie M. 2018. Meta-Analysis of the association between GABA receptor polymorphisms and autism spectrum disorder (ASD). *Journal of Molecular Neuroscience* **65**:1–9. DOI: https://doi.org/10.1007/s12031-018-1073-7, PMID: 29725984

Maksay G. 1994. Thermodynamics of gamma-aminobutyric acid type A receptor binding differentiate agonists from antagonists. *Molecular Pharmacology* **46**:386–390. DOI: https://doi.org/10.1007/BF00168633, PMID: 8078501

Masiulis S, Desai R, Uchański T, Serna Martin I, Laverty D, Karia D, Malinauskas T, Zivanov J, Pardon E, Kotecha A, Steyaert J, Miller KW, Aricescu AR. 2019. GABA_A receptor signalling mechanisms revealed by structural pharmacology. *Nature* **565**:454–459. DOI: https://doi.org/10.1038/s41586-018-0832-5, PMID: 30602790

McKernan RM, Farrar S, Collins I, Emms F, Asuni A, Quirk K, Broughton H. 1998. Photoaffinity labeling of the benzodiazepine binding site of alpha1beta3gamma2 gamma-aminobutyric acidA receptors with flunitrazepam identifies a subset of ligands that interact directly with His102 of the alpha subunit and predicts orientation of these within the benzodiazepine pharmacophore. *Molecular Pharmacology* **54**:33–43. DOI: https://doi.org/10.1124/mol.54.1.33, PMID: 9658187

Mellor JR, Randall AD. 1997. Frequency-dependent actions of benzodiazepines on GABAA receptors in cultured murine cerebellar granule cells. *The Journal of Physiology* **503 (Pt 2**:353–369. DOI: https://doi.org/10.1111/j.1469-7793.1997.353bh.x, PMID: 9306278

Möhler H, Fritschy JM, Rudolph U. 2002. A new benzodiazepine pharmacology. *Journal of Pharmacology and Experimental Therapeutics* **300**:2–8. DOI: https://doi.org/10.1124/jpet.300.1.2

Nayak TK, Vij R, Bruhova I, Shandilya J, Auerbach A. 2019. Efficiency measures the conversion of agonist binding energy into receptor conformational change. *Journal of General Physiology* **151**:465–477. DOI: https://doi.org/10.1085/jgp.201812215

Nemecz Ákos, Prevost MS, Menny A, Corringer P-J. 2016. Emerging Molecular Mechanisms of Signal Transduction in Pentameric Ligand-Gated Ion Channels. *Neuron* **90**:452–470. DOI: https://doi.org/10.1016/j.neuron.2016.03.032

O'Shea SM, Williams CA, Jenkins A. 2009. Inverse effects on gating and modulation caused by a mutation in the M2-M3 linker of the GABA(A) receptor gamma subunit. *Molecular Pharmacology* **76**:641–651. DOI: https://doi.org/10.1124/mol.109.055111, PMID: 19553237

O'Shea SM, Harrison NL. 2000. Arg-274 and Leu-277 of the γ-Aminobutyric Acid Type A Receptor α2 Subunit Define Agonist Efficacy and Potency. *Journal of Biological Chemistry* **275**:22764–22768. DOI: https://doi.org/10.1074/jbc.M001299200

Olfson M, King M, Schoenbaum M. 2015. Benzodiazepine use in the United States. *JAMA Psychiatry* **72**:136–142. DOI: https://doi.org/10.1001/jamapsychiatry.2014.1763, PMID: 25517224

Olsen RW, Sieghart W. 2008. Subtypes of gamma-aminobutyric acid(A) receptors: classification on the basis of subunit composition, pharmacology, and function. *Pharmacological Reviews* **60**:243–260.

Perrais D, Ropert N. 1999. Effect of zolpidem on miniature IPSCs and occupancy of postsynaptic GABAA receptors in central synapses. *The Journal of Neuroscience* **19**:578–588. DOI: https://doi.org/10.1523/JNEUROSCI.19-02-00578.1999, PMID: 9880578

Pflanz NC, Daszkowski AW, Cornelison GL, Trudell JR, Mihic SJ. 2018. An intersubunit electrostatic interaction in the GABAA receptor facilitates its responses to benzodiazepines. *Journal of Biological Chemistry* **293**:8264–8274. DOI: https://doi.org/10.1074/jbc.RA118.002128

Phulera S, Zhu H, Yu J, Claxton DP, Yoder N, Yoshioka C, Gouaux E. 2018. Cryo-EM structure of the benzodiazepine-sensitive α1β1γ2s tri-heteromeric GABA_A receptor in complex with GABA. *eLife* **7**:e39383. DOI: https://doi.org/10.7554/eLife.39383, PMID: 30044221

Pless SA, Sivilotti LG. 2018. A tale of ligands big and small: an update on how pentameric ligand-gated ion channels interact with agonists and proteins. *Current Opinion in Physiology* **2**:19–26. DOI: https://doi.org/10.1016/j.cophys.2017.12.012

Pritchett DB, Sontheimer H, Shivers BD, Ymer S, Kettenmann H, Schofield PR, Seeburg PH. 1989. Importance of a novel GABAA receptor subunit for benzodiazepine pharmacology. *Nature* **338**:582–585. DOI: https://doi.org/10.1038/338582a0, PMID: 2538761

Purohit P, Gupta S, Jadey S, Auerbach A. 2013. Functional anatomy of an allosteric protein. *Nature Communications* **4**:2984. DOI: https://doi.org/10.1038/ncomms3984, PMID: 24352193

Purohit P, Auerbach A. 2009. Unliganded gating of acetylcholine receptor channels. *PNAS* **106**:115–120. DOI: https://doi.org/10.1073/pnas.0809272106, PMID: 19114650

Ramamoorthi K, Lin Y. 2011. The contribution of GABAergic dysfunction to neurodevelopmental disorders. *Trends in Molecular Medicine* **17**:452–462. DOI: https://doi.org/10.1016/j.molmed.2011.03.003, PMID: 21514225

Rogers CJ, Twyman RE, Macdonald RL. 1994. Benzodiazepine and beta-carboline regulation of single GABAA receptor channels of mouse spinal neurones in culture. *The Journal of Physiology* **475**:69–82. DOI: https://doi.org/10.1113/jphysiol.1994.sp020050, PMID: 7514665

Rudolph U, Möhler H. 2014. GABAA receptor subtypes: therapeutic potential in down syndrome, affective disorders, schizophrenia, and autism. *Annual Review of Pharmacology and Toxicology* **54**:483–507. DOI: https://doi.org/10.1146/annurev-pharmtox-011613-135947, PMID: 24160694

Rüsch D, Forman SA. 2005. Classic benzodiazepines modulate the Open–Close Equilibrium in α1β2γ2L γ-Aminobutyric Acid Type A Receptors. *Anesthesiology* **102**:783–792. DOI: https://doi.org/10.1097/00000542-200504000-00014

Scheller M, Forman SA. 2002. Coupled and uncoupled gating and desensitization effects by pore domain mutations in GABA(A) receptors. *The Journal of Neuroscience* **22**:8411–8421. PMID: 12351715

Schmitz A. 2016. Benzodiazepine use, misuse, and abuse: a review. *Mental Health Clinician* **6**:120–126. DOI: https://doi.org/10.9740/mhc.2016.05.120

Sieghart W, Sperk G. 2002. Subunit composition, distribution and function of GABA(A) receptor subtypes. *Current Topics in Medicinal Chemistry* **2**:795–816. DOI: https://doi.org/10.2174/1568026023393507, PMID: 12171572

Sigel E. 2002. Mapping of the benzodiazepine recognition site on GABA(A) receptors. *Current Topics in Medicinal Chemistry* **2**:833–839. DOI: https://doi.org/10.2174/1568026023393444, PMID: 12171574

Sigel E, Ernst M. 2018. The benzodiazepine binding sites of GABA$_A$ Receptors. *Trends in Pharmacological Sciences* **39**:659–671. DOI: https://doi.org/10.1016/j.tips.2018.03.006, PMID: 29716746

Sigel E, Lüscher BP. 2011. A closer look at the high affinity benzodiazepine binding site on GABAA receptors. *Current Topics in Medicinal Chemistry* **11**:241–246. DOI: https://doi.org/10.2174/156802611794863562, PMID: 21189125

Smart TG, Stephenson FA. 2019. A half century of γ-aminobutyric acid. *Brain and Neuroscience Advances* **3**: 239821281985824. DOI: https://doi.org/10.1177/2398212819858249

Solís-Añez E, Delgado-Luengo W, Hernández ML. 2007. Autism, chromosome 15 and the GABAergic dysfunction hypothesis. *Investigacion Clinica* **48**:529–541. PMID: 18271397

Steinbach JH, Akk G. 2019. Applying the Monod-Wyman-Changeux allosteric activation model to Pseudo-Steady-State responses from GAB$_{AA}$ Receptors. *Molecular Pharmacology* **95**:106–119. DOI: https://doi.org/10.1124/mol.118.113787, PMID: 30333132

Tasneem A, Iyer LM, Jakobsson E, Aravind L. 2004. Identification of the prokaryotic ligand-gated ion channels and their implications for the mechanisms and origins of animal Cys-loop ion channels. *Genome Biology* **6**:R4. DOI: https://doi.org/10.1186/gb-2004-6-1-r4, PMID: 15642096

Venkatachalan SP, Czajkowski C. 2012. Structural link between γ-Aminobutyric acid type A (GABAA) Receptor agonist binding site and inner β-Sheet governs channel activation and allosteric drug modulation. *Journal of Biological Chemistry* **287**:6714–6724. DOI: https://doi.org/10.1074/jbc.M111.316836

Vicini S, Mienville JM, Costa E. 1987. Actions of benzodiazepine and beta-carboline derivatives on gamma-aminobutyric acid-activated Cl- channels recorded from membrane patches of neonatal rat cortical neurons in culture. *The Journal of Pharmacology and Experimental Therapeutics* **243**:1195–1201. PMID: 2447266

Vien TN, Modgil A, Abramian AM, Jurd R, Walker J, Brandon NJ, Terunuma M, Rudolph U, Maguire J, Davies PA, Moss SJ. 2015. Compromising the phosphodependent regulation of the GABAAR β3 subunit reproduces the core phenotypes of autism spectrum disorders. *PNAS* **112**:14805–14810. DOI: https://doi.org/10.1073/pnas.1514657112, PMID: 26627235

Wagner DA, Czajkowski C. 2001. Structure and dynamics of the GABA binding pocket: a narrowing cleft that constricts during activation. *The Journal of Neuroscience* **21**:67–74. DOI: https://doi.org/10.1523/JNEUROSCI.21-01-00067.2001, PMID: 11150321

Walters RJ, Hadley SH, Morris KD, Amin J. 2000. Benzodiazepines act on GABAA receptors via two distinct and separable mechanisms. *Nature Neuroscience* **3**:1274–1281. DOI: https://doi.org/10.1038/81800, PMID: 11100148

Wyman J, Gill S. 1990. *Binding and Linkage: Functional Chemistry of Biological Macromolecules.* University Science Books. DOI: https://doi.org/10.1016/0014-5793(91)81192-B

Zhu S, Noviello CM, Teng J, Walsh RM, Kim JJ, Hibbs RE. 2018. Structure of a human synaptic GABAA receptor. *Nature* **559**:67–72. DOI: https://doi.org/10.1038/s41586-018-0255-3